

# Characterizing and Optimizing Photocathode Laser Distributions for Ultra-low Emittance Electron Beam Operations\*

F. Zhou,\*\* D. Bohler, Y. Ding, S. Gilevich, Z. Huang, H. Loos, D. Ratner, and S. Vetter

*SLAC National Accelerator Laboratory, 2575 Sand Hill Road, Menlo Park, CA 94025, USA*

Photocathode RF gun has been widely used for generation of high-brightness electron beams for many different applications. The drive laser distributions in such RF guns play important roles in minimizing the electron beam emittance. Characterizing the laser distributions with measurable parameters and optimizing beam emittance versus the laser distribution parameters in both spatial and temporal directions are highly desired for high-brightness electron beam operation. In this paper, we report systematic measurements and simulations of emittance dependence on the measurable parameters represented for spatial and temporal laser distributions at the photocathode RF gun systems of Linac Coherent Light Source. The tolerable parameter ranges for photocathode drive laser distributions in both directions are presented for ultra-low emittance beam operations.

PACS number: 29.27.-a, 42.55.-f

## I. INTRODUCTION

The performance of x-ray free electron lasers (FELs) [1-5] depends critically on the emittance of the electron beam. The electron beam is typically generated from an RF gun, and further accelerated to high energy with one or two stages of longitudinal bunch compression. The final beam emittance at the undulator can be impacted by collective effects through acceleration and bunch compression, but it is dominated by the initial emittance from the RF gun, especially the time-sliced emittance which is important for FEL performance. There are thermionic RF guns being adopted in FEL [2], but the most popular RF guns [1,3-5] are based on laser driven photocathode, from which the generated electron bunch could have lower emittance, lower energy spread and flexibility of bunch length control. For example, at the Linac Coherent Light Source (LCLS), a typical electron bunch from the photo-injector would have an emittance about  $0.4 \mu\text{m}$ , a sliced energy spread  $\sim 1 \text{ keV}$ , and a bunch length about  $0.5 \text{ mm rms}$  for  $180\text{-}250 \text{ pC}$ .

Optimizing photo-injector for achieving low-emittance electron beam is an important subject. Photo-injector source emittance is mostly dominated by: photocathode thermal emittance, space-charge force induced emittance, and transverse radio frequency (RF) kick induced emittance [6-7]. The space-charge effect is sensitive to the photocathode drive laser parameters. Extensive studies have been performed in the past decades to mitigate the space charge effect [7-12]. While the linear space-charge forces can be compensated by well-known solenoid focusing [8], the nonlinear space-charge forces (e.g. from nonuniform quantum efficiency distribution [7]) are more complicated. With the laser-driven photo-injector, one can manipulate the laser distribution to minimize the nonlinear space charge forces. For example, an ellipsoidal electron distribution would only have linear space-charge force which in principle can be completely compensated [10-11]. However, generation of ellipsoidal laser pulse is challenging. Studies also show that the emittance can be improved with a relatively simpler laser distribution, spatial truncated-Gaussian, which has been successfully implemented at the LCLS [12].

As discussed above, the electron beam quality can be optimized with manipulation of the drive laser. However, it is challenging to maintain a constant desired laser distribution for 24/7 operating laser systems. For example, the laser distributions are susceptible to external environment changes such as humidity and temperature, and also laser-related maintenance work. Thus, it is highly desirable to characterize somehow-complicated photocathode laser shape with

measurable parameters, and study the parameter tolerances for maintaining ultra-low emittance, which can guide the laser scientists to recover laser distributions within desired ranges after laser maintenance work. This study performed at the LCLS injector can be directly adapted to other similar X-FEL facilities, such as Pohang X-FEL [4] and Swiss X-FEL [3].

In this paper, we report electron beam emittance dependence on the laser spatial and temporal distributions based on simulations and measurements at the LCLS. A truncated-Gaussian spatial laser distribution is being used for this study and detailed characterization and optimization are discussed. This paper is organized as follows. Section II will introduce the measures of the laser spatial distribution and emittance dependence on the parameters for drive laser spatial distributions. In Section III the emittance dependence on the temporal laser distribution/parameters is presented. The tolerable laser parameter ranges for ultra-low emittance are summarized in Section IV.

## II. MEASURING AND OPTIMIZING THE SPATIAL LASER DISTRIBUTION

At the LCLS, the drive laser system is a frequency tripled, chirped-pulse amplification system based on aTi:sapphire laser. The system consists of mode-locked oscillator, followed by a pulse stretcher oscillator, a regenerative amplifier, two multi-pass amplifiers, pulse compressor, and finally a frequency tripler to convert the IR laser to 253-nm ultraviolet beam. The 253-nm laser beam is finally delivered to the copper photocathode through a long in-vacuum transport from the laser room on the ground to the 10-m deep SLAC linac tunnel.

Many previous studies showed that the photocathode drive laser with a uniform distribution in spatial dimensions produces a lower emittance beam. However, recent simulations and experimental observations at the LCLS show that the truncated-Gaussian spatial laser beam produces a better emittance beam than uniform laser does. This is because the space charge is more linear with truncated-Gaussian laser than uniform one, resulting in better emittance compensation [12]. Figure 1 (top) shows the different spatial lineout distributions including pseudo-uniform (a), truncated-Gaussian (b), and Gaussian-like (c). The projected and time-sliced emittances of three distributions are simulated, as shown in Fig. 1 (bottom), using ImpactT code [13] for 150 pC. The emittance with the spatial truncated-Gaussian distribution improves  $\sim 30\%$  in comparison to the pseudo uniform laser or Gaussian-like one.

Generating and maintaining the desired spatial truncated-Gaussian laser beam on the photocathode, however, is not trivial for 24/7 operational laser systems. Thus, we need to understand what the laser distributions are tolerated for high-brightness electron beam. For example, what range of  $g/h$  (the ratio of the top Gaussian part height to bottom hard edge height shown in Fig.1 (top, b)) is tolerated for ultra-low emittance? Simulations also show the unbalanced hard edge heights  $a1$  and  $a2$  shown in Fig. 2 (top) may increase the emittance, as shown in Fig. 2 (bottom). According to the simulations, the best emittance can be obtained with hard edge height  $a1=a2$ . But in practice, the balanced hard edge height may become unbalanced after long period of operation. So, what ratio of  $a1/a2$  can be tolerable for the high-brightness electron beam? Thus, having quantitative measures for laser distributions becomes highly needed for characterizing, optimizing and controlling the spatial laser beam shapes for ultra-small emittance beam.

First, we need to develop methods to effectively characterize spatial laser distributions as measurable parameters. In the following sub-sections we describe two major measures, spatial laser lineout distribution and laser Zernike modes [14] of the spatial laser shapes. Then, we discuss the emittance dependence on these measurable parameters. When the laser on the photocathode has regular smooth spatial distribution, either of two measures can characterize laser beam shapes. However, in practical, the laser distribution is sometimes irregular from the laser systems and transports due to misalignment and mirror damages. In such a case, using lineout distribution parameter may not fully represent a true laser beam, and thus a better characterization method would be needed. The parameters for laser Zernike modes are found as a better measure of the spatial laser distributions for this case, although the method is more complicated. With two vital measures, the desired parameters for spatial laser distribution can be measured and maintained within the tolerable ranges for ultra-low emittance beam generation.

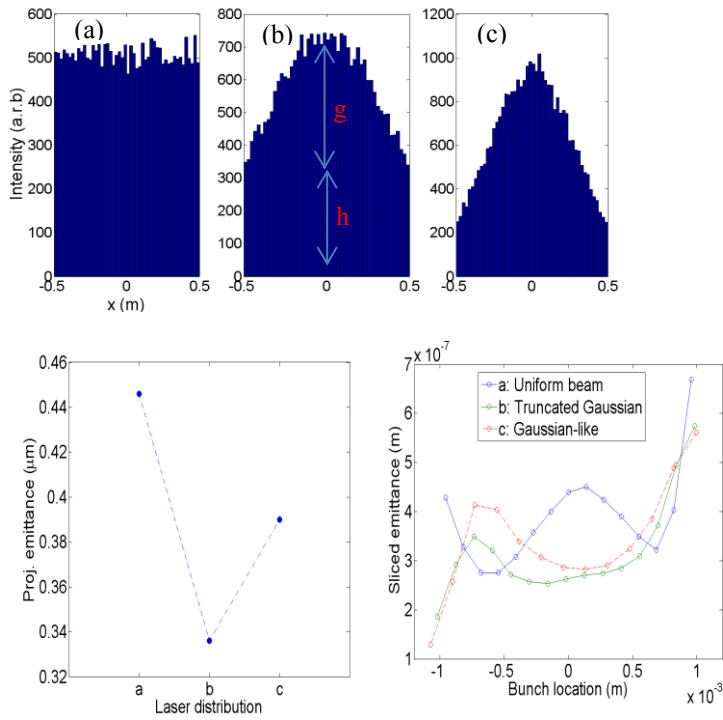


FIG.1. Spatial laser lineout distributions (top), (a), (b) and (c) represent pseudo uniform, certain truncated-Gaussian and Gaussian-like spatial distributions; corresponding projected (bottom, left) and slice emittances (bottom, right) for 150 pC.

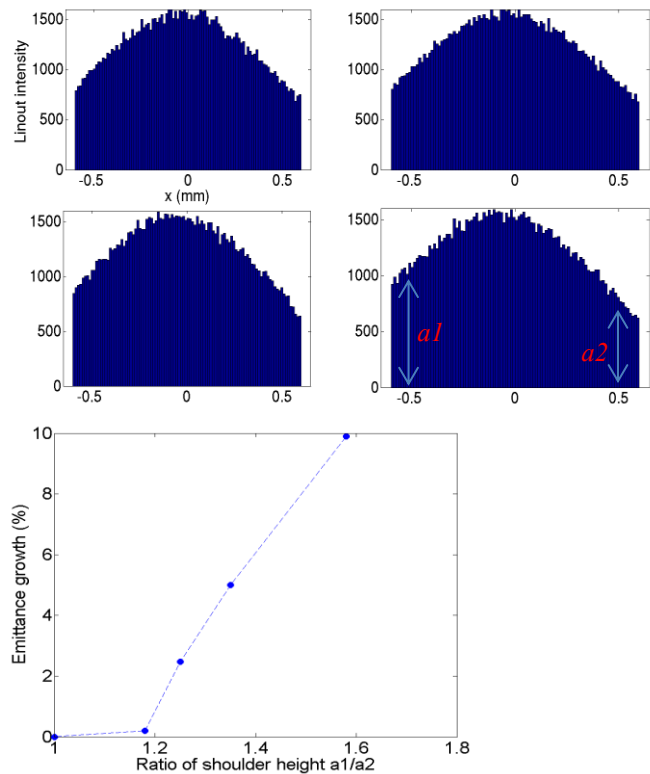


FIG. 2. Line-out distribution with unbalanced laser hard edge heights  $a_1$  and  $a_2$  (top), and emittance growth as function of  $a_1/a_2$  (bottom) for 150 pC.

## A. Parameterized with laser lineout distribution and emittance dependence on the parameters

When the spatial laser distribution is reasonably smooth, as in the example shown in Fig. 3, using lineout-distribution is a simple way to quantify laser distribution. The lineout intensity ratio  $g/h$  shown in Fig.3 is used to determine the laser shape. The laser is pseudo uniform with  $g/h < 0.1$ , while it is near Gaussian distribution with  $g/h > 3$ . Figure 4 shows both simulated (left) and measured (right) emittance for different  $g/h$  with 150 pC. Both measurements and simulations show that the optimum emittance is achieved with  $g/h \sim 1$ . Measurements with aid of simulations indicate that emittance growth can be maintained below 10% with  $g/h$  ranged within 0.5-1.5. For a regular smooth-like spatial Gaussian laser beam, the lineout intensity ratio  $g/h$  can be adjusted within the desired range using an optical telescope before the iris at the LCLS injector laser systems.

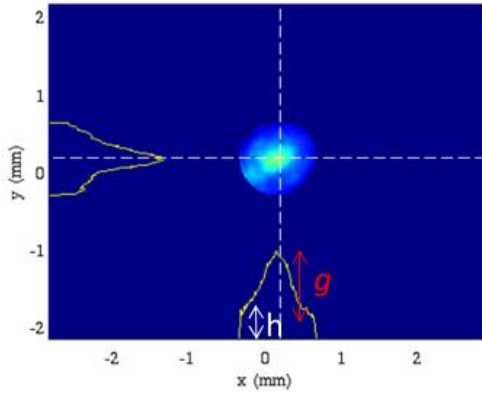


FIG.3. Example of regular smooth photocathode laser distribution parameterized by the lineout intensity ratio  $g/h$ .

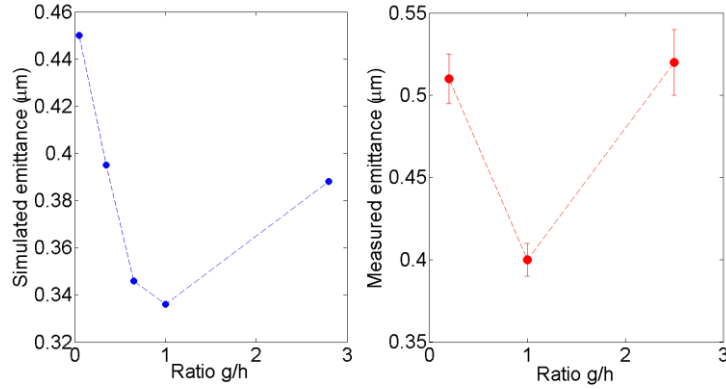


FIG.4. Simulated (left) and measured (right) emittance for different  $g/h$  of lineout intensity ratio for 150 pC.

## B. Parameterized with laser Zernike modes and emittance dependence on the parameters

The spatial photocathode laser distribution can be characterized by a more powerful method, Zernike modes (or polynomials), although the method is complicated. Zernike functions are widely used in the optical systems to characterize the measured structures of deformations and aberrations, because these form a complete, orthogonal basis over the unit circle. The Zernike functions are a product of the Zernike radial polynomials and sine- and cosine-functions [15]:

$$\begin{cases} Z_n^m(r, \theta) \\ Z_n^{-m}(r, \theta) \end{cases} = R_n^m(r) \begin{cases} \sin m\theta \\ \cos m\theta \end{cases} \quad (1)$$

The index  $n=0, 1, 2, \dots$  is called the degree of the polynomial, while  $m=-n$  to  $+n$ , with  $(n-m)$  even, is called the order. Radial polynomial  $R(r)$  is usually defined as sum of power of  $r$ :

$$R_n^m(r) = \sum_{k=0}^{(n-m)/2} \frac{(-1)^k (n-k)!}{k! \left(\frac{n+m}{2} - k\right)! \left(\frac{n-m}{2} - k\right)!} r^{n-2k} \quad n=0, 1, 2, \dots, (n-m) \text{ even} \quad (2)$$

As they are orthogonal over the unit circle, these function  $Z_n^m(r, \theta)$  can be used to decompose complex function  $f(r, \theta)$ :

$$f(r, \theta) = \sum_p a_p Z_p(r, \theta), \quad (3)$$

where  $a_p$  is the coefficient for Zernike modes. Therefore, any function (or laser shape) defined on the circle can be expressed as a sum of Zernike modes.

At the LCLS, laser images were used to numerically compute the Zernike coefficients  $a_p$ . The coefficients are used to reconstruct the laser images and identify the relative contribution of each mode. Two parameters that were defined using the Zernike Coefficients are used to quantify the actual laser distribution [16]. Namely, the symmetry power ( $p_{\text{sym}}$ ) is calculated by summing the squares of the  $m=0$  coefficients. The asymmetry power ( $p_{\text{asym}}$ ) is determined by summing the squares of the remaining mode coefficients. Figure 5 shows one example of the first twenty-one Zernike modes  $Z_n^m$  [14], where  $n=0$  to  $5$ , and  $m=-n$  to  $+n$  with  $(n-m)$  even. In the LCLS experiment, the first fifty-one modes were used to achieve reasonable-resolution for image reconstruction. For pseudo-uniform and symmetrical Gaussian-like laser distributions in this study their symmetry powers are  $p_{\text{sym}} < 1\%$  and  $p_{\text{sym}} > 7\%$ , respectively. When laser is symmetry in both  $x$ - and  $y$ -plane, the asymmetry power  $p_{\text{asym}}$  is  $< 1\%$ .

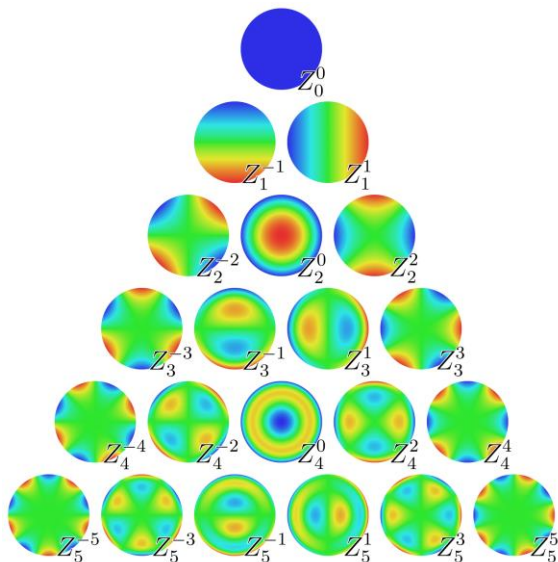


FIG. 5: Example of twenty-one Zernike modes  $Z_n^m$ .

Figure 6 shows three different laser images illuminated on the LCLS cathode (top, a-c) and the emittance dependence on their relevant symmetry power  $p_{\text{sym}}$  (bottom) for 150 pC with fixed asymmetry power  $p_{\text{asym}} < 1\%$ . The experimental data shows that the ultra-small emittance can be maintained with the symmetry power  $p_{\text{sym}}$  in within 2.5%-4% (i.e., truncated Gaussian distributions). Figure 7 shows the measured emittance dependence on the laser beam asymmetry

power, for a fixed  $p_{\text{sym}}=2.5\%$ . The measurement shows the emittance growth can be controlled  $<5\%$  with the  $p_a < 1.5\%$ .

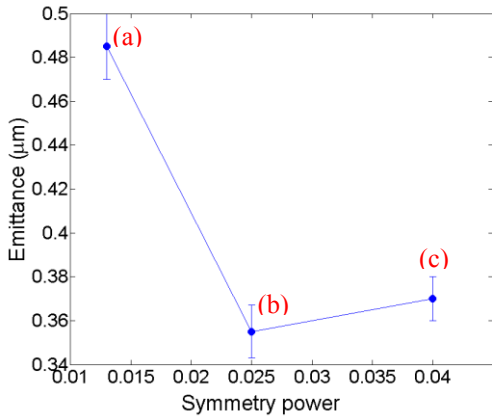
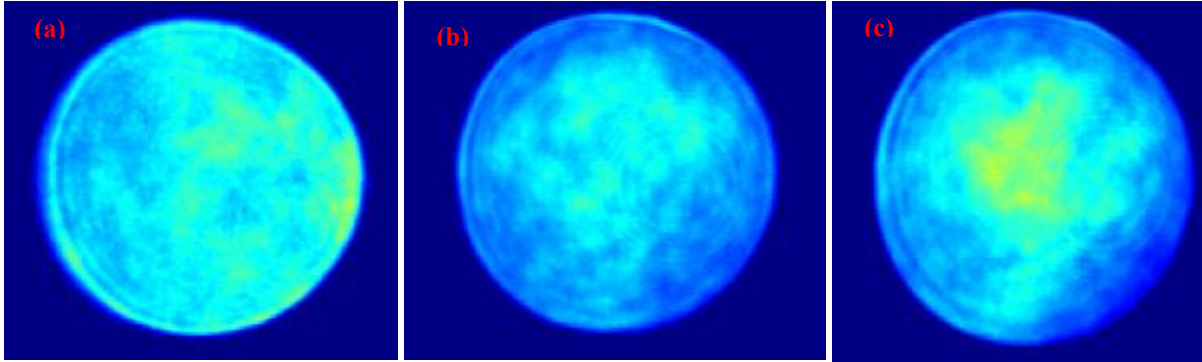


FIG.6. Photocathode laser shapes; measured emittance vs. symmetry power relevant to three laser shapes with fixed asymmetry  $p_{\text{asym}} < 1\%$ .

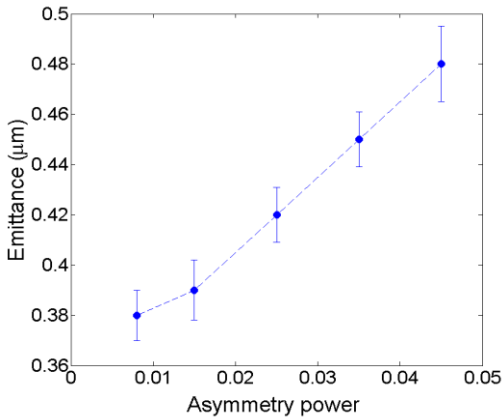


FIG.7. Measured emittance dependence on the asymmetry power for a fixed  $p_{\text{sym}}=2.5\%$ .

### III. OPTIMIZATIONS OF TEMPORAL LASER DISTRIBUTION

RF kick induced emittance  $\epsilon_{rf}$  and space charge emittance  $\epsilon_{sc}$  strongly depends on the photocathode drive laser pulse length [6], expressed by:

$$\epsilon_{rf} \sim E \cdot \sigma_r^2 \cdot \sigma_z^2 \quad (4)$$

$$\varepsilon_{sc} \sim \frac{Q}{E \cdot \sigma_z} \mu_x \quad (5)$$

where  $E$  is the peak accelerating gradient on cathode,  $\mu_x$  is the transverse space charge factors related to the aspect ratio of the rms beam size  $\sigma_r$  to rms bunch length  $\sigma_z$ , and  $Q$  is the bunch charge. Eqs. 4 and 5 indicate that the laser pulse length has to be traded off between space charge force and RF kick emittance for an optimum emittance. Systematic simulations of the emittance dependence on the single Gaussian temporal laser length are performed for 180 pC, as shown in Fig. 8. It shows that the projected (left) and sliced emittances (right) are nearly in optimum with a single  $\sim 3.5$  ps FWHM Gaussian laser.

Current LCLS drive laser pulse is  $2.0 \pm 0.2$  ps FWHM in length. For the current LCLS drive laser systems it's difficult to lengthen laser pulse length  $> 3$  ps FWHM without compromising the temporal laser profile. Instead, two  $\sim 2$  ps s- and p-polarization Gaussian lasers are stacked together to lengthen the laser pulse length. The advantages using pulse stacking over single Gaussian laser: 1) flexible to adjust overall laser pulse length for various needs; 2) relatively sharper edges (or faster rise/fall time) of the laser pulse for better emittance compensation process. As shown in Fig. 8, a better projected emittance is simulated with a stacked  $\sim 4$  ps FWHM pulse ( $\sim 2$  ps separation for stacking two 2-ps pulses) than a single 3.5 ps FWHM Gaussian laser, although their slice emittance is similar. This is confirmed that the 4 ps stacked pulse has better emittance compensation than single 3.5 ps Gaussian due to relatively faster rise/fall time.

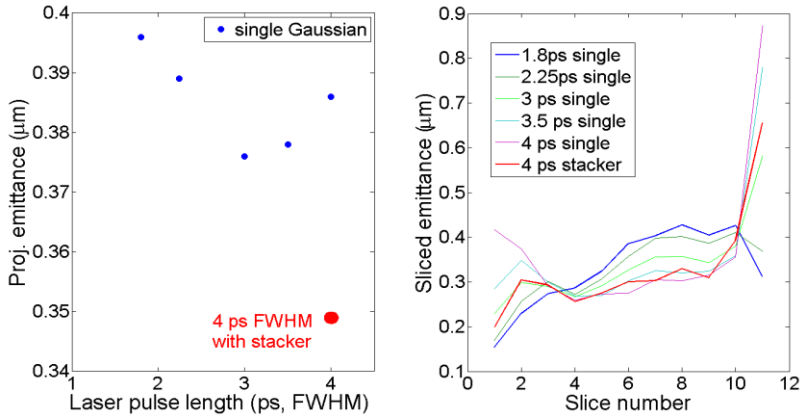


FIG.8. Simulated projected (left) and sliced (right) emittance dependence on a single Gaussian laser and a stacked pulse 4 ps FWHM for 180 pC.

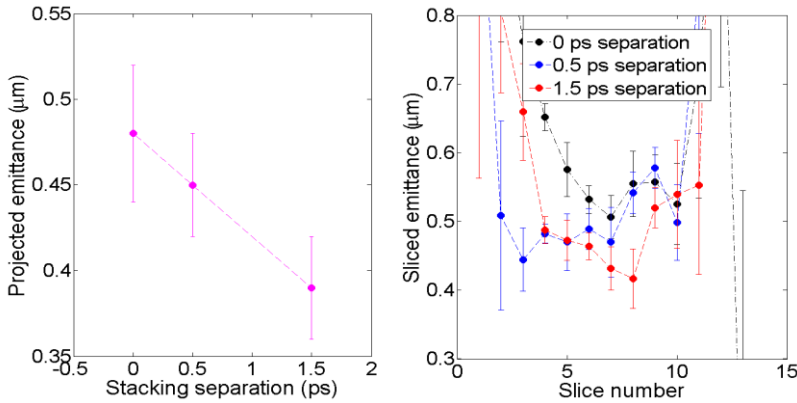


FIG.9. Measured projected (left) and slice (right) emittance (250 pC) with different pulse separation for stacking two  $\sim 2$  ps FWHM pulses.

Figure 9 shows the comparison of the measured projected (left) and sliced (right) emittance for single ~2 ps Gaussian and stacked two 2-ps laser pulses. The projected emittance is measured with one wire scanner at the LCLS injector. The details of emittance measurements are described in Ref. [17]. The measured projected emittance is significantly improved with 1.5 ps separation of the pulse stacking compared with single 2 ps Gaussian (i.e., overlapping the s-polarized with p-polarized pulse). Simulations and measurements show the emittance can be slightly further improved with the separation up to 2 ps. But we chose 1.5-ps separation for LCLS operations to avoid some parasitic effects in longitudinal dimension due to a longer initial bunch. The slice emittance is measured with an S-band transverse deflector and an OTR screen at the injector with the laser heater chicane turned-off [17]. The measured slice emittance trend shows the emittance is improved with 1.5 ps separation of the pulse stacking, in comparison to single Gaussian 2-ps laser for 250 pC. During the emittance measurements shown in Fig. 8, the spatial laser profile on the cathode may be not optimized for optimum emittance but kept unchanged for fair comparisons. The stacked laser pulse eventually improves the x-ray FEL pulse intensity by 30-50% compared with single Gaussian ~2 ps FWHM laser pulse.

#### IV. SUMMARY

Characterizing and controlling transverse laser distribution on the photocathode with measurable parameters is highly desired for maintaining ultra-low emittance beam at the LCLS. Quantitative measurements of the laser parameters represented for spatial distribution using lineout distribution and Zernike polynomials are developed. According to measurements with simulations, ultra-low emittance can be established and maintained with truncated-Gaussian spatial laser distribution, of  $g/h$  in between 0.5-1.5 using lineout distribution method, or of symmetry power in between 2.5%-4% using Zernike modes method. The emittance dilution can be controlled below 10% with ratio of laser hard edge heights  $a1/a2 < 1.5$ . Measurements and simulations also indicate that an ultra-small emittance can be achieved with either a single Gaussian of 3.5 ps FWHM or stacked laser pulse of about 4 ps FWHM for 180-250 pC. These quantified criteria for spatial and temporal laser distributions, may guide to recover laser distributions within the desired ranges for maintaining high-brightness x-ray FEL operation. These results are not only useful for LCLS injector but also for similar X-FEL injectors such as SWISS X-FEL and Pohang X-FEL injectors.

\* The work is supported by DOE under grant No. DE-AC02-76SF00515.

\*\* [zhoufeng@slac.stanford.edu](mailto:zhoufeng@slac.stanford.edu)

#### REFERENCES

- [1] P. Emma *et al.*, „first lasing and operation of an Angstrom-wavelength free electron laser“, *Nature Photon.* 4 641 (2010).
- [2] T. Ishikawa *et al.*, „A compact x-ray free electron laser emitting in the sub-angstrom region“, *Nature Photonics* 6, 540-544 (2012).
- [3] H. H. Braun, „SWISSFEL, the X-ray Free Electron Laser at PSI“, *Proceedings of FEL2012*, Nara, Japan.
- [4] H.-S. Kang, K.W.Kim, I.S.Ko, „Status of the PAL XFEL construction“, *Proceedings of IPAC2015*, Richmond, VA, USA.
- [5] K. Honkavaara, B. Faatz, J. Feldhaus, S. Schreiber, R. Treusch, M. Vogt, *Proceedings of FEL2013*, New York, NY, USA.
- [6] K-J. Kim, *Nucl. Instrum. Methods Phys. Res. Sect. A* 275, 201 (1989).
- [7] F. Zhou, I. Ben-Zvi, M. Babzien, X. Chang *et al.*, “Experimental characterization of emittance growth induced by the nonuniform transverse laser distribution in a photoinjector”, *Phys. Rev. ST-AB* 5, 094203 (2002).

- [8] B. Carlsten, “New photoelectric injector design for the LOS Alamos National Laboratory XUV FEL Accelerator”, Nucl. Instr. Methods A285, 313 (1989).
- [9] J. Gallardo and R. Palmer, “emittance correction of photocathode gun”, Nucl. Instr. Methods A304 (1991) 345-347.
- [10] P. Piot *et al.*, “Formation and acceleration of uniformly filled ellipsoidal electron bunches obtained via space charge driven expansion from a cesium-telluride photocathode”, Phys. Rev. ST Accel. Beams 16, 010102 (2013).
- [11] M. Bakr, M. Khojayan, M. Krasilnikov, F. Stephan, G. Vaschenko, “Beam dynamics simulation for the upgraded PITZ photocathode laser pulse shapes”, Daejeon, South Korea, FEL15
- [12] F. Zhou, A. Brachmann, P. Emma, S. Gilevich, and Z. Huang, “Impact of the spatial laser distribution on photocathode gun operation”, Phys. Rev. ST-AB 15, 090701 (2012).
- [13] J. Qiang, ImpactT code manual, LBNL-62326, 2007.
- [14] Zernike function see link below: [https://en.wikipedia.org/wiki/Zernike\\_polynomials](https://en.wikipedia.org/wiki/Zernike_polynomials)
- [15] P. Fricker, analysing lasik optical data using Zernike functions, <http://www.mathworks.com/company/newsletters/articles/analyzing-lasik-optical-data-using-zernike-functions.html>
- [16] D. Bohler, LCLS physics meeting, 2013.
- [17] F. Zhou, K. Bane, Y. Ding, Z. Huang, H. Loos, and T. Raubenhemier, “Measuring and analysis of a high-brightness electron beam collimated in a magnetic bunch compressor”, Phys. Re. ST-AB 18, 050702 (2015).